Int J Adv Manuf Technol (2009) 45:459–469
DOI 10.1007/s00170-009-1988-9

ORIGINAL ARTICLE

Investigation of the viscous and thermal effects on ductile fracture in sheet metal blanking process

Ahmad Rafsanjani · Saeed Abbasion · Anoushiravan Farshidianfar · Nilgoon Irani

Received: 9 July 2008 / Accepted: 18 February 2009 / Published online: 10 March 2009

Abstract In this paper, a methodology is proposed to predict the ductile damage in the sheet metal blanking process using a coupled thermomechanical finite-element method. A constitutive material model combined with the ductile fracture criteria was used. The effect of material softening due to the heat generated during plastic work in a specimen was considered in blanking simulations. To verify the validity of the proposed model, several blanking simulations are performed and the results compared with those obtained from an experimental study. The interaction of fracture initiation and temperature distribution in the sheet metal during the process was studied. The effect of velocity and the clearance on the product shape were examined. It was seen that at high punch speeds the viscous and thermal effects have significant effects on product quality.

Keywords Blanking · Thermal · Viscous · FEM

A. Rafsanjani (✉)
Member of Young Researchers Club of Islamic Azad University, Tehran-Center Branch,
Tehran, Iran
e-mail: rafsanjani@mecheng.iust.ac.ir

S. Abbasion
Department of Mechanical Engineering,
Iran University of Science and Technology,
Tehran, Iran

A. Farshidianfar
Department of Mechanical Engineering,
Ferdowsi University of Mashhad,
Mashhad, Iran

N. Irani
Department of Mechanical Engineering,
Amir Kabir University of Technology,
Tehran, Iran

Nomenclature

$\overline{\varepsilon}_p$	effective plastic strain
$\dot{\overline{\varepsilon}}$	effective strain rate
$\overline{\sigma}$	flow stress
σ_1	maximum tensile stress
σ_h	hydrostatic stress
A_G	Goijaerts criterion constant
A_{RT}	Rice and Tracey criterion constant
A_O	Oyane criterion constant
B_G	Goijaerts criterion constant
C_i	critical damage values
T	temperature

1 Introduction

Sheet metal blanking process is one of the most widely used manufacturing processes. The complex nature of this process involving separation and material fracture makes the design and realization of the metal blanking process an empirical effort. As a result, the appropriate process settings must be determined by time-consuming trial and error, and uncontrollable variations in product dimension often still arise during production. Finite-element technique is an appropriate method to take over the restrictions of the process simulation. Due to improvement of computational resources, the blanking simulation has been developed considerably in recent years and many researchers devoted their consideration to study this process in details.

The early works on numerical simulation of the blanking process has been done by Lee et al. [1]. They studied the rigid-plastic analysis of the fine-blanking process with the finite-element method. Faura et al. [2] proposed a methodology to predict the optimum punch–die clearance accord-

ing to the direction of crack propagation. Brokken et al. [3] presented a numerical model using an arbitrary Lagrange Euler method combined with remeshing to describe the large deformations in the process. Ductile fracture is also incorporated in this model by a discrete crack approach. Samuel [4] performed a finite-element analysis and derived the work-hardening behavior of the material from a relationship between the equivalent plastic strain, the equivalent Von Mises stress, and the Vickers hardness in the shear zone. Chen et al. [5] conducted a numerical computation of strain localization in the fine-blanking process. It was seen that the high strain localization on clearance zone leads to localized plastic flow which may cause the initiation of shear bands. Pyttel et al. [6] presented a finite-element model for description of aluminum sheet metal blanking based on ideas of fracture mechanics. Maiti et al. [7] used a finite-element technique to study the influence of tool clearance, friction, sheet thickness, punch–die size and blanking layout on the sheet deformation. Klocke et al. [8] developed a finite-element code to study both blanking and fine-blanking processes. This includes prediction of crack initiation using various rupture criteria and investigation of the effect of clearance and friction on the product shape. Fang et al. [9] investigated the effect of punch–die clearance on the forming quality of the aluminum blanked parts. Rachik et al. [10] performed an experimental and numerical study on sheet metal blanking process. The presented numerical model is based on a dynamic explicit scheme. An arbitrary Lagrange Euler formulation is also used in this model for adaptive meshing. Aoki and Takahashi [11] established an analysis method by applying the Fourier phase correlation method to the viscoplasticity method for obtaining accurate material flow and strain distribution in a short time in a sheet metal blanking process. Klingenberg and Singh [12] presented a methodology towards the development of a system for the online characterization of the blank material during the blanking process.

The above review clearly indicates that such problems are of considerable interest in a variety of practical applications. For example, in the manufacturing of some parts of a car seat belt lock, the quality of the blanked parts has a great influence on the product performance. Figure 1 shows different parts of seat belt lock produced with blanking process.

The blanking process is a shearing operation which involves elastic and plastic deformation, punch penetration, and ductile fracture [2]. The physical background for ductile fracture initiation in metals is well understood from the sequential mechanisms of initiation, growth, and coalescence of voids [13]. The fracture mechanics assumptions based on the presence of an initial crack and considering its growth are not sufficient to describe the blanking process precisely. The alternative fracture model that has been used for blanking and other shearing simulation is the local approach to fracture [14]. In this method, the attention is focused on a single material point. An attempt is made to predict failure at this point by considering the history of the local state variables. As a consequence, an impressive number of fracture criteria based on the local approach to fracture have been proposed which has been used in many research works to study the metal blanking process. Goijaerts et al. [15] predicted both punch force and fracture initiation for blanking of a ferritic stainless steel in various blanking geometries based on the finite-element method, employing a rate-dependent elasto-

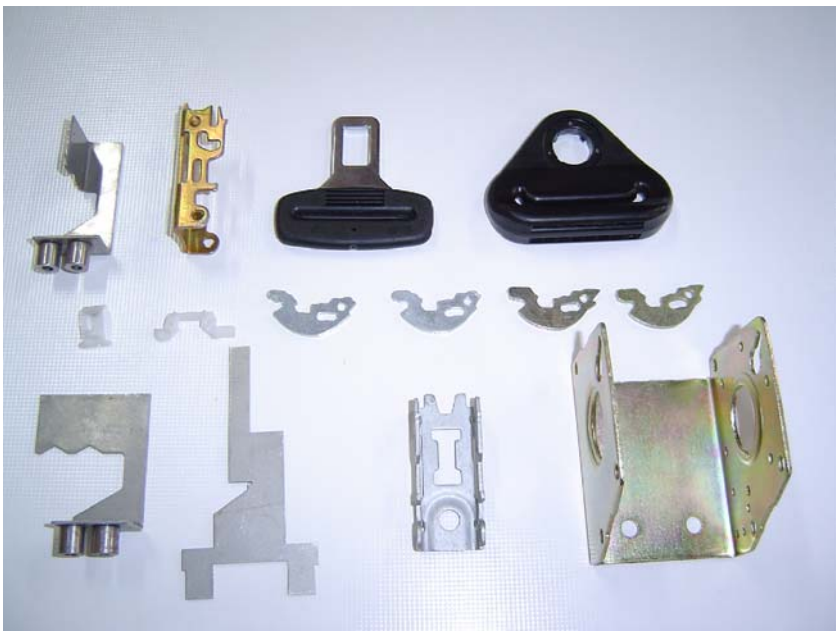

Fig. 1 Seat belt parts produced by blanking process in TAHA GHALEB TOOS company

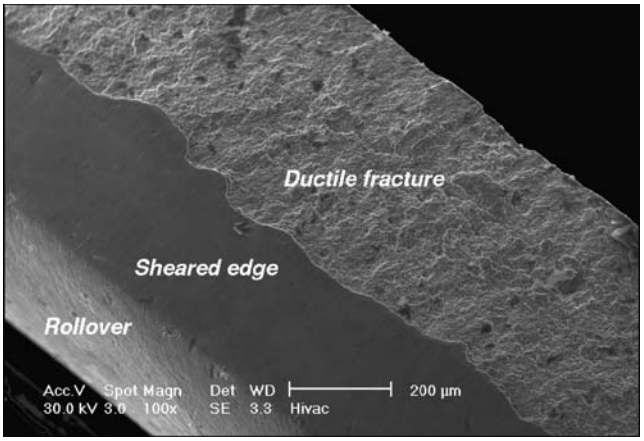

Fig. 2 Product edge, picture by permission of Prof. F. P. T Baaijens and Prof. H. E. H. Meijer

plastic constitutive model combined with a fracture criterion. Hambli and Reszka [16] identified the critical values of various fracture criteria in order to simulate crack initiation and propagation generated by shearing mechanisms. Shim et al. [17] applied Cockroft and Latham [18] criterion using a finite-element technique for simulation of a blanking operation of an aluminum foil and a copper foil. Komori [19] studied the effect of various ductile fracture criteria on crack initiation and propagation during the shearing operation. Yu et al. [20] presented a new fracture criterion combined with modified Brozzo [21] criteria and effective strain criteria using a trial and error procedure so that the value of the breaking might have the same value as the experiment.

Plastic deformation and contact friction during the blanking process causes a temperature gradient which makes the blanking process a coupled thermomechanical problem. However, according to the authors' knowledge, in only a few studies has the effect of multiphysical coupling been taken into account. Brokken [5] studied temperature distributions in sheet metals for different punch velocities but left fracture out of consideration. Lestriez et al. [22] studied the multiphysical coupling in metal forming using a finite-element model. This study focused on the coupling between thermal exchange, small strain elasticity, and finite plasticity with nonlinear hardening, ductile damage, and contact with friction. Chen et al. [23] investigated the tearing failure in a fine-blanking process using a coupled thermomechanical finite-element method.

The primary purpose in most of blanking simulations is to predict the punch force and the product shape. The blanked edge consists of four distinct zones: rollover, sheared, fractured zone, and burr. The objective of blanking designers is to increase the sheared zone and decrease the others. Ideally, blanked parts have no fracture, rollover, and burr zone and almost completely sheared. Figure 2 shows the blanked edge zones.

In this paper, the sheet metal blanking process was simulated using DEFORM2D, a commercial finite-element code. The effect of material softening due to heat generation because of plastic deformation was introduced to the simulation using a coupled thermomechanical finite-element method. The effect of punch speed and punch–die clearance on blanking quality was carefully examined. To verify the proposed model, a selection of predicted product shapes was compared to experimental data and the validity of the work was checked.

2 Material model

In industrial practice, blanking is often performed at high punch velocities. This causes significant thermal and viscous effects in the material behavior. The flow stress of a metal under uniaxial conditions can be described as a function of strain, strain rate, and temperature:

$$\overline{\sigma} = \overline{\sigma}\left(\overline{\varepsilon}_{\mathrm{p}}, \dot{\overline{\varepsilon}}, T\right) \tag{1}$$

Where $\overline{\sigma}$ is the flow stress; $\overline{\varepsilon}_{\mathrm{p}}$is the effective plastic strain; $\dot{\overline{\varepsilon}}$ is the effective strain rate, and T is the temperature.

In this paper, a chrome stainless steel X13Cr30 is employed for sheet material. The flow stress for different strain rates and temperatures is determined experimentally in the form of a table by Goijaerts. A graphical representation is given in Fig. 3.

3 Ductile fracture

Failure in the blanking process usually occurs as ductile fracture when the voids of microscale grow up. Figure 4 is a microscopic image of X30Cr13 sheet which is showing a ferrite matrix with carbide inclusions and Fig. 5 is the

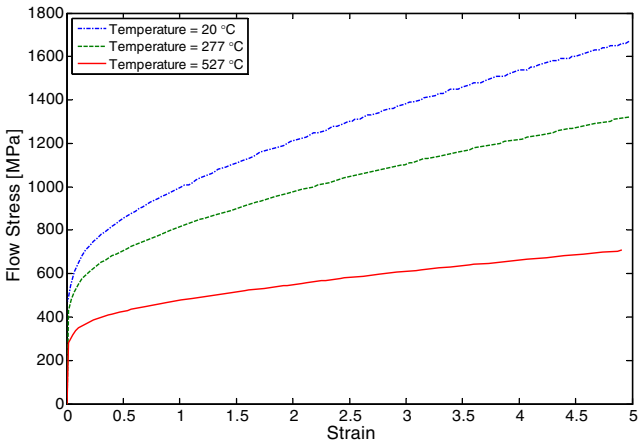

Fig. 3 Strain hardening curves from Goijaerts [27] for strain rate of 0.001 per second

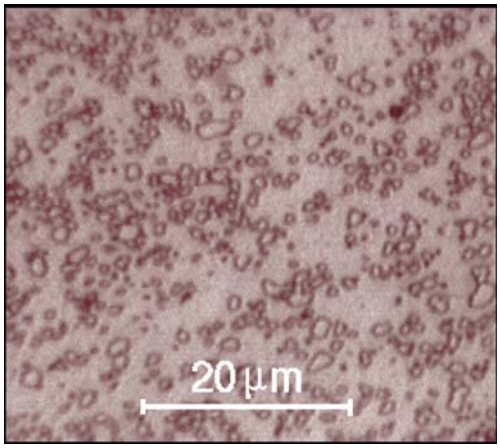

Fig. 4 Microscopic image of a polished and etched sheet X30Cr13, showing a ferrite matrix with carbide inclusions [13]

fractured edge of a blanked sheet. In the local approach to fracture, the ductile fracture occurs in three stages: nucleation, growth, and coalescence. The microscopic holes which are generally initiated by imperfections in the matrix material in the vicinity of second-phase particles results in nucleation. The voids can grow due to plastic deformation for which the rate of the growth is affected by deformation history and the stress applied. The hydrostatic part of the stress has a strong influence on the growth rate. Under the influence of plastic deformation, the voids can grow until a number of voids coalesce to initiate a crack. The local criteria for ductile fracture can be generally represented by the following functional form:

$$\int_{\bar{\varepsilon}_p} f(\sigma)\, \mathrm{d}\bar{\varepsilon}_p = C_0 \tag{2}$$

Where $\bar{\varepsilon}_p$ is the effective plastic strain and C_0 is the critical damage value. The value of C_0 can be calculated experimentally. Different types of ductile fracture criteria which are given empirically are listed in the following.

The energy or generalized plastic work criterion is given first by Freudenthal [24]

$$\int_{\bar{\varepsilon}_p} \bar{\sigma}\, \mathrm{d}\bar{\varepsilon}_p = C_1 \tag{3}$$

Where $\bar{\sigma}$ and $\bar{\varepsilon}_p$ are the equivalent (Mises) stress and strain, respectively.

Rice and Tracey [25] suggested the fracture criterion including the effect of hydrostatic stress σ_h in the following exponential form:

$$\int_{\bar{\varepsilon}_p} \exp\left(A_{RT}\frac{\sigma_h}{\sigma_1}\right) \mathrm{d}\bar{\varepsilon}_p = C_2 \tag{4}$$

Oyane et al. [26] also considered hydrostatic stress σ_h in their criterion

$$\int_{\bar{\varepsilon}_p} \left(1 + A_O\frac{\sigma_h}{\bar{\sigma}}\right) \mathrm{d}\bar{\varepsilon}_p = C_3 \tag{5}$$

Cockcroft and Latham [18] fracture criterion states that the fracture in a ductile material occurs when

$$\int_{\bar{\varepsilon}_p} \sigma_1\, \mathrm{d}\bar{\varepsilon}_p = C_4 \tag{6}$$

Where σ_1 is the maximum tensile stress and $\bar{\varepsilon}_p$ is the effective strain. The Cockcroft and Latham criterion was modified by Brozzo et al. [21] to introduce the effect of hydrostatic stress σ_h in an explicit form in order to correlate their experimental results:

$$\int_{\bar{\varepsilon}_p} \frac{2}{3}\frac{\sigma_1}{\sigma_1 - \sigma_h}\mathrm{d}\bar{\varepsilon}_p = C_5 \tag{7}$$

Goijaerts [27] suggested a new model to predict ductile fracture initiation in both blanking and tensile testing

$$\int_{\bar{\varepsilon}_p} \left(1 + A_G\frac{\sigma_h}{\bar{\sigma}}\right) \bar{\varepsilon}_p^{B_G}\mathrm{d}\bar{\varepsilon}_p = C_6 \tag{8}$$

In this section, various criteria are introduced to predict ductile fracture in the sheet metal blanking process. Some of these criteria have been investigated to be more suitable for the simulation of the blanking process. By considering the viscous and thermal effects in the blanking simulation, the problem becomes more complicated. As mentioned in previous sections, an increase in temperature will cause a decrease of the actual yield stress. Due to thermal conduction at low-speed blanking, the heat generated during plastic work in the material will not cause a significant local temperature change. But at high punch

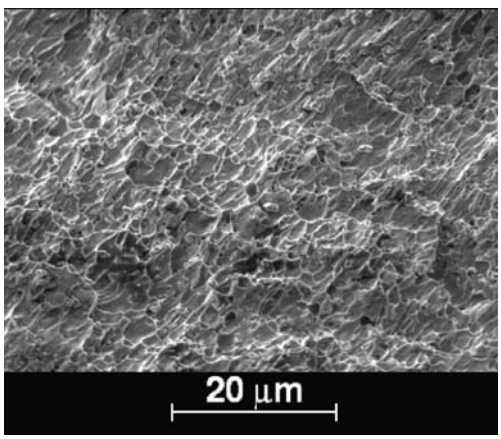

Fig. 5 SEM image of dimples on the fractured edge of a blanked sheet X30Cr13. The shear is directed from the *lower left corner* towards the upper right corner of the image [13]

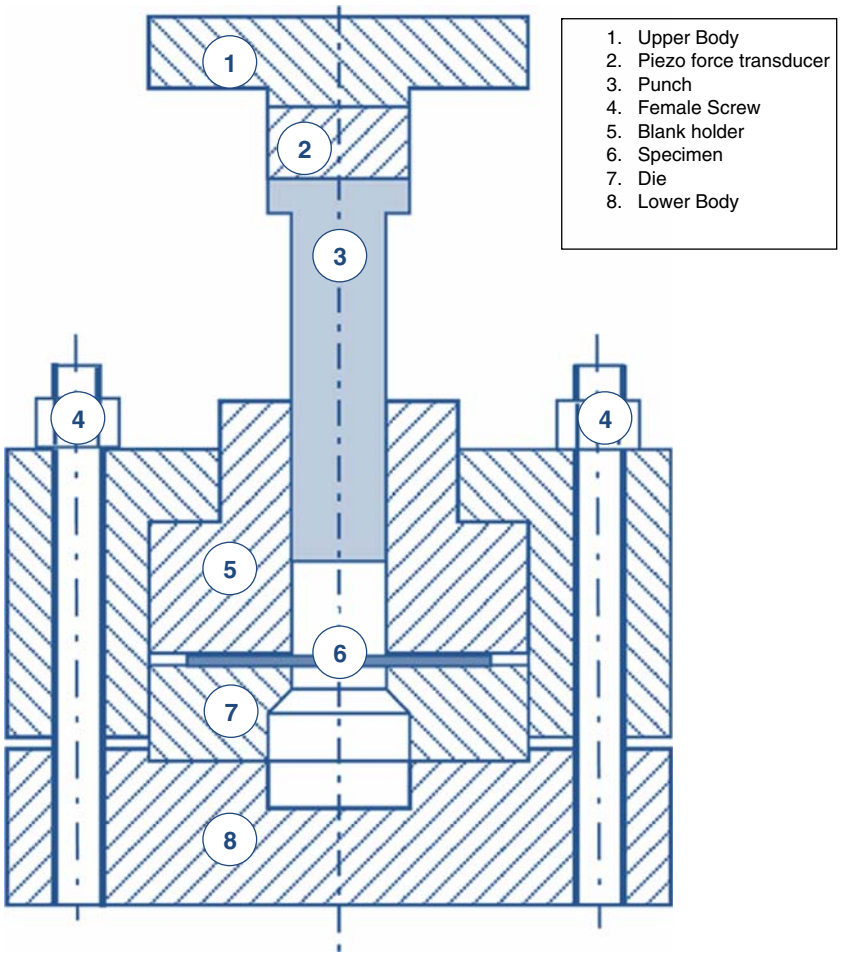

Fig. 6 Axisymmetric blanking setup of experiments performed by Goijaerts

speeds, the local increase of temperature particularly at the fracture zone results in a local drop of actual yield stress.

4 Axisymmetric blanking setup

The blanking experiment was performed using an axisymmetric setup which is built into a hydraulic tensile testing machine. The ductile fracture initiation can be measured after the blanking process. This setup allows us to perform experiments at high blanking speeds. The measurement of the characteristics of the blanked edge for various blanking speed, which is largely determined by ductile fracture initiation, is reported by Goijaerts [27].

The setup is schematically shown in Fig. 6. Different clearances S were realized by the application of different punches. Due to limitations in manufacturing accuracy, the individual punch radii are not exactly identical. Table 1 specifies the geometrical parameters of blanking setup. The sheet material is a ferritic 13% chrome stainless steel X13Cr30 which is common in industrial applications and is mostly used in cutting devices such as shavers.

5 Finite-element simulation

The blanking process was simulated using a commercial finite-element program called the DEFORM2D [28]. The simulation is based on a rigid-plastic finite-element method. Various ductile fracture criteria can be applied to the model which predicts the fracture initiation with the element kill method. This simulation makes it possible to investigate the properties of the sheared surface in the blanking process [29]. The material properties of chrome steel X30Cr13 are specified in Table 1 and the geometrical parameters of the

Table 1 Geometrical parameters used for the simulation

Tools	Diameter	Cutting Radius	Clearance
Die	10.00	0.136	–
Punch 1	9.98	0.082	0.01
Punch 2	9.94	0.088	0.03
Punch 3	9.88	0.086	0.06
Punch 4	9.80	0.098	0.10
Punch 5	9.70	0.088	0.15

Table 2 Material parameters of X30Cr13

Properties	Values
Young's modulus	1.87×10^5 MPa
Poisson's ratio	0.28
Yield strength	420 MPa
Thermal conductivity	50 W/m K
Friction coefficient	0.1

experimental setup reported in Table 2 are considered for blanking simulation. Various simulations with different geometries and blanking speeds have been carried out and the results of the simulation are discussed in the following sections.

Quadrilateral elements were used for simulation in which the meshes around the fracture zone were refined in three levels. Figure 7 illustrates the blanking process for 10% clearance in the finite-element scheme. Up to 4,500 elements were used to construct the finite-element model and automatic remeshing was employed to avoid nonproper meshes. To apply an axisymmetric boundary condition, the left boundary of the model was chosen for the axis of symmetry and the other boundaries are left free except for contacting surfaces.

6 Verification of the proposed model

In this section, a representative of the experimental results selected to examine the validity of the coupled thermomechanical finite-element model is used for the blanking simulation. The blanking simulation is performed for different clearances and punch speeds for chrome steel X30Cr13. The adopted Rice and Tracey criterion is used for the simulation of ductile fracture. The critical damage value, C_2, for X30Cr13 in this criterion was measured experimentally by Goijaerts et al. [30] to be 2.76 and A_{RT} equals to 2.9.

6.1 Blanking force

The blanking force is calculated during the punch stroke for the three sizes of punch–die clearance. The conventional blanking simulations overestimate the punch loads slightly by approximately 5% [27]. In these methods, the material softening due to the heat generation during the blanking process was not taken into account. However, a coupled thermomechanical finite-element model can describe this process in more detail. The results of the simulation for the calculation of the blanking force are plotted in Fig. 8 and compared with data reported from the same experiments by Mediavilla et al. [31]. Figure 8a shows the force–displacement curves and Fig. 8b is a comparison of the maximum punch force between simulation results and experimental data. This comparison shows good agreement between simulation results and experimental data and verifies the validity of the proposed model for prediction of the blanking force.

6.2 Product shape

In any blanking simulation, the prediction of product shape is of great interest. Goijaerts [27] measured the length of

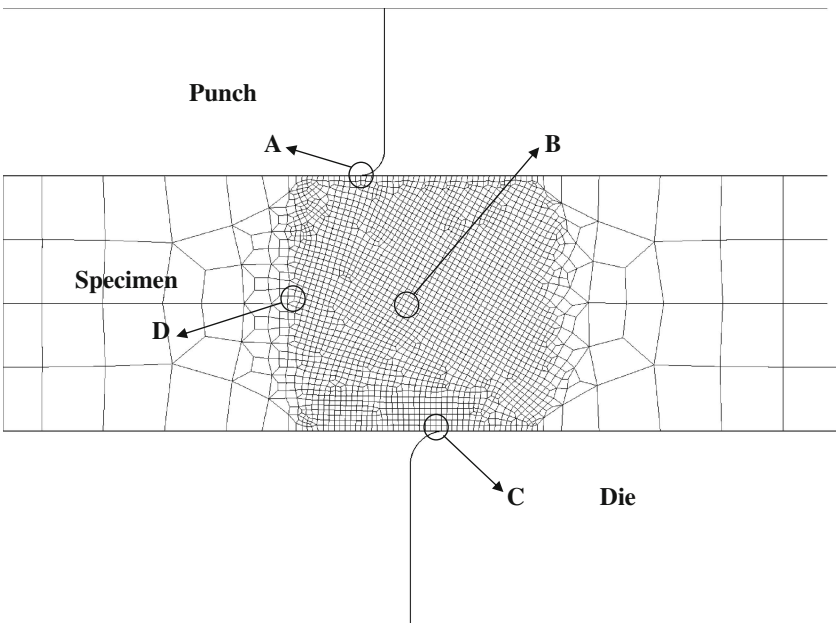

Fig. 7 Finite-element model of blanking process for 10% clearance

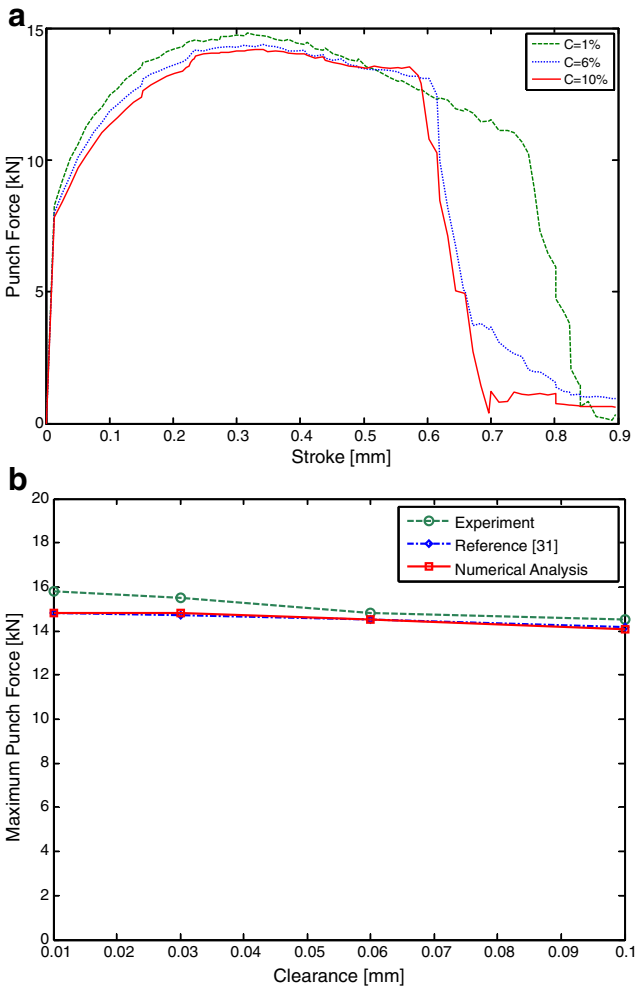

Fig. 8 **a** Blanking displacement–force curves for different clearances. **b** A comparison of maximum punch force for different clearances between simulation results and experimental data

the sheared edge L_S on the sheet and the height of the burr L_B on the blank for different clearances. The size of rollover L_R was recovered from finite-element analysis. Figure 9 shows the definition of characteristic lengths L_S,

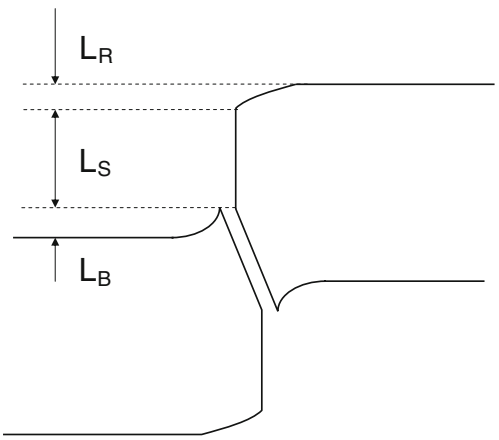

Fig. 9 Definition of characteristic lengths

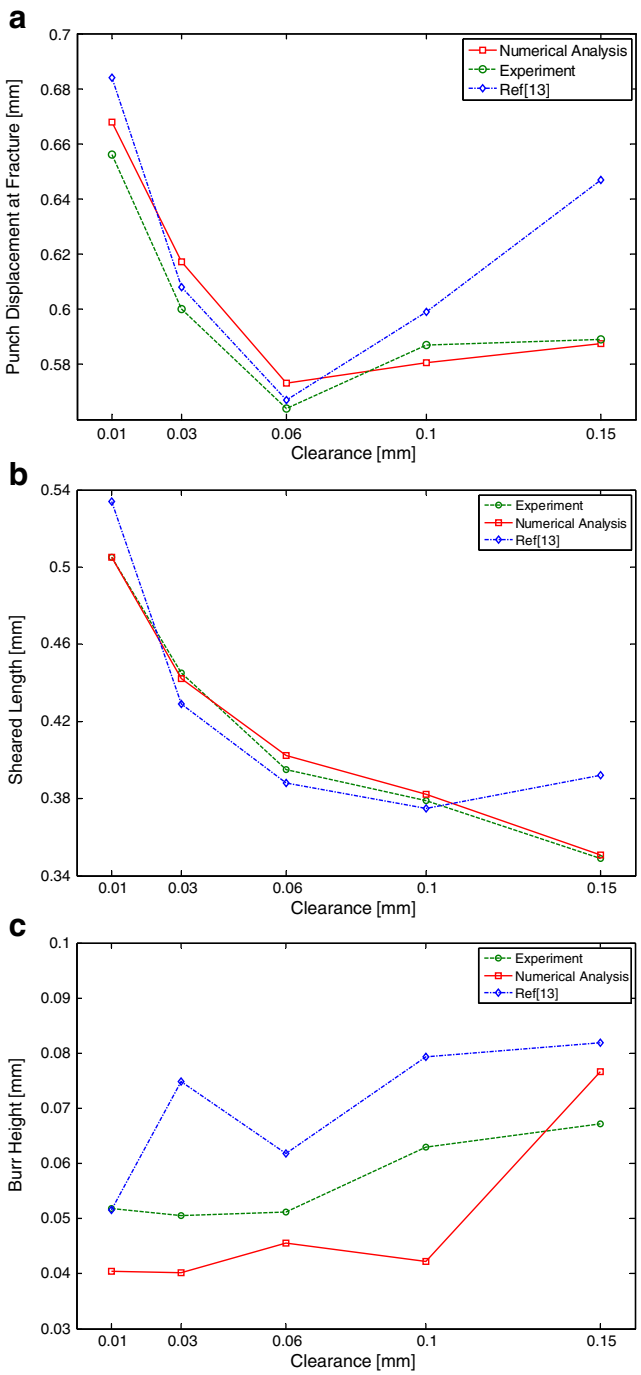

Fig. 10 **a** Punch displacement at fracture. **b** Length of sheared edge on sheet. **c** Size of the burr on the blank

L_B, and L_R. In this section, the estimated lengths for different clearances are compared with experimental data [27] and numerical results reported by Brokken [13]. Figure 10a shows the punch displacement at fracture; Fig. 10b shows the length of sheared edge on the sheet and Fig. 10c shows the size of the burr on the blank. This comparative study between the numerical simulations and the experiments verifies the simulated results.

7 Results and discussion

The blanking process is simulated using a two-dimensional, axisymmetric, thermomechanically coupled finite-element model. The model geometries are assumed to be in accordance with the experimental setup for five different clearances. The analysis performed for different punch speeds and the influence of blanking speed and thermal effects on the product shape were investigated.

At high punch velocities, viscous and thermal effects in the material behavior are not negligible. To overcome this limitation, it is necessary to define the time-dependent behavior of material as described in "Section 2." The proposed model allows the simultaneous application of remeshing and fracture criterion so that the temperature distribution during fracture initiation can be estimated. Figure 11 describes the maximum temperature of a specimen for different clearances and velocities at fracture initiation. At low punch speeds, the temperature gradient in the specimen is not noticeable but at high punch speeds the temperature rises sharply in the fracture zone as the clearance decreases. Figure 12 shows the temperature variation of sheet metal under the punch radius as the punch penetrates into the sheet metal on the right axis and blanking forces on the left axis versus time. It can be seen that the maximum temperature of the specimen is related to the fracture initiation in the specimen. After fracture initiates, the temperature decreases.

The evolution of the temperature with respect to the imposed displacement for some selected points in the specimen also was examined. Point A is located at the intersection of the punch radius and the specimen; point B is at the middle of the line that connects the center of the curvature of the punch and the die radiuses; point C is the contact point of the sheet and the die radius and finally point D is located outside of the shear band. Figure 13 shows the temperature evolution at these points. The temperature increases similarly in four points at the early stage of plastic deformation. The temperature increases rapidly and simultaneously in three points (A, B, and C) located inside the shear bands. However, it increases much less in point D outside the bands where elastic unloading takes place. When the first damage localization takes places at the shear bands, the temperature at point A increases rapidly to reach T_{max}=63.9°C and decreases when the microscopic crack initiates at this point. Points B and C have similar behavior to point A. At these three points, the temperature decreases slightly when the elastic unloading takes place in point D after the formation of localized necking. The temperature of point D increases until the specimen is fractured completely and after that decreases sharply. All four points reach the same temperature. According to the above observation, one can

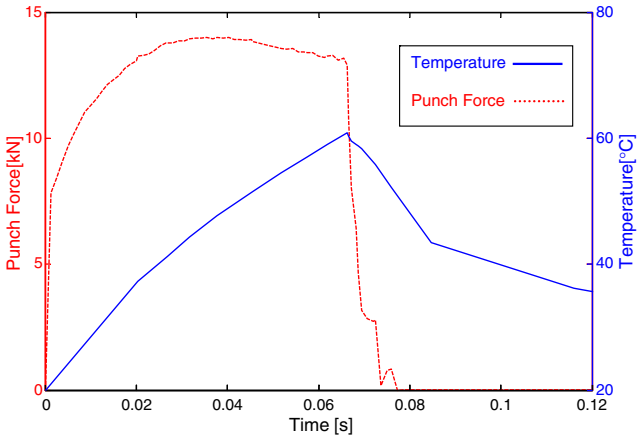

Fig. 12 Blanking force and sheet temperature under the punch radius versus time for C=10% and v=10 mm/s

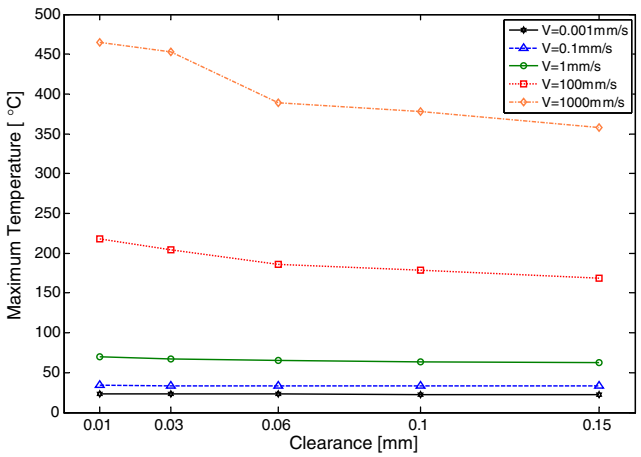

Fig. 11 Influence of punch speed on max temperature of the specimen

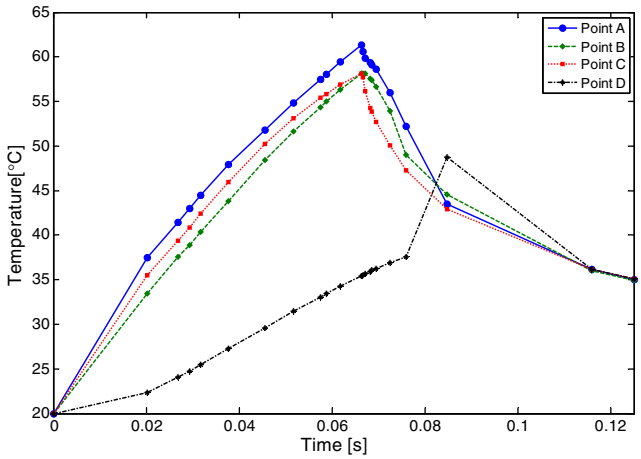

Fig. 13 Temperature variations of some selected points in fracture zone

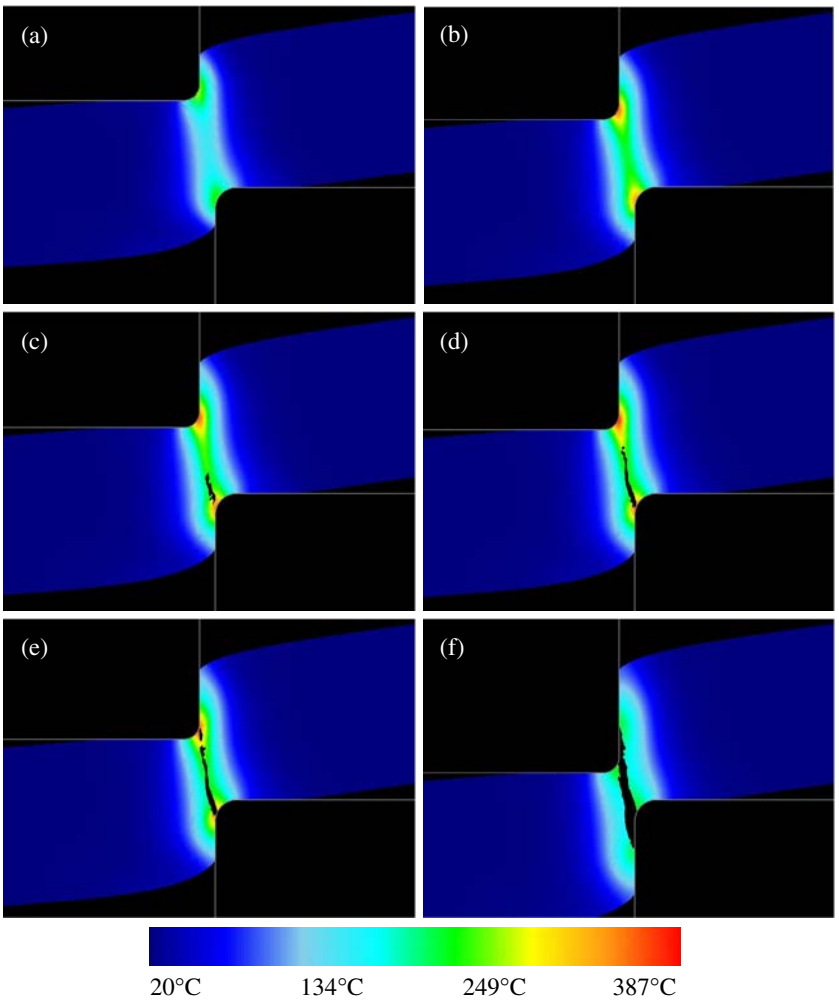

Fig. 14 Temperature distributions in specimen at different fracture stages during blanking process for C=10% and v= 1,000 mm/s

conclude that the fracture initiates at the maximum temperature in each stroke while the growth and coalescence of voids occur almost at constant temperature near the maximum temperature. Consequently, the ductile fracture is influenced indirectly by the temperature gradient in the material and the punch velocity through the rate-dependent constitutive material model introduced in "Section 2." Figure 14 shows the temperature distribution

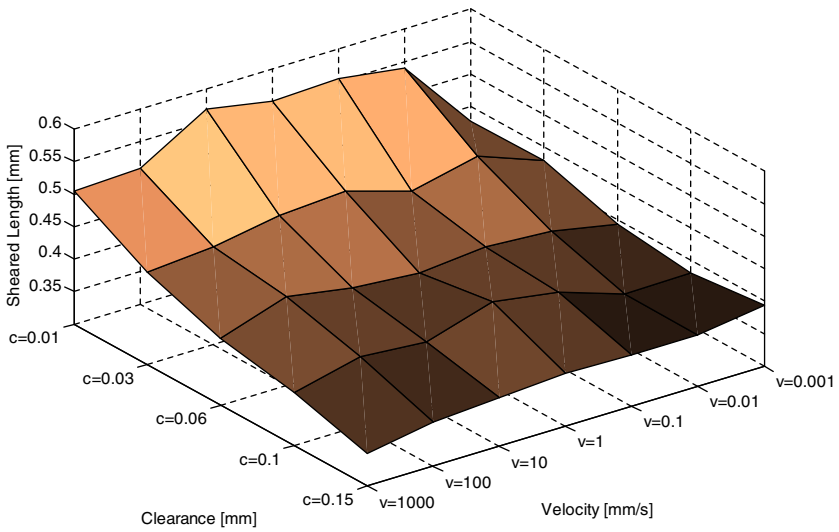

Fig. 15 Effect of clearance and velocity on length of sheared edge

in a specimen at different fracture stages during the blanking process. In this simulation, the clearance is set to be 10% and punch speed is 10 mm/s. It can be seen that during the blanking process the fracture initiation and crack growth occur at the maximum temperature. To study the effect of both velocity and clearance on product shape, a 3D surface is plotted in Fig. 15. In this figure, the shear length is plotted with respect to clearance and velocity. It is shown that the shear length is not influenced by the punch speed up to 10 mm/s but for high punch speeds the shear length decreases sharply. It can be explained by thermal effects. Because of thermal softening due to the temperature rise in the deformation zone, the local stresses decrease and the deformation will become more localized. This localization results in extra heat generation in the specimen which causes earlier fracture initiation and smaller shear length. So, at high punch speeds, the shear zone is smaller than low punch speeds. It also can be detected that the length of the shear zone is influenced by both clearance and velocity; so, for different purposes, the clearance and the velocity of the blanking process should be selected correctly. Figure 15 also indicates that at small punch clearances the shear zone may be small. In this case, the sheared zone may be torn which affects the edge quality.

8 Conclusion remarks

In this work, the blanking process is simulated using a coupled thermomechanical finite-element model. The present work is concerned with the thermomechanical behavior of sheet metal during the blanking process. A series of finite-element simulations were performed and the results of the simulations were compared with an experimental study. This comparison shows good agreement between the simulated results and the experimental data. The interaction of fracture initiation in the specimen and the temperature distribution was studied in detail. This study shows that the fracture initiates at the maximum temperature during the process and after the fracture takes place the temperature decreases sharply. The present study explains multiphysical coupling in the blanking simulation which has not been considered before. From the current study, it can be concluded that, at high punch speeds, viscous and thermal effects have considerable effects on product quality and must be taken into account.

Acknowledgment The authors wish to thank Prof. F. P. T Baaijens and Prof. H. E. H Meijer for their technical support. We also thank Dr. A. M. Goijaerts for providing valuable experimental data. The research work was supported by the Taha Ghaleb Toos research group of Mashhad, Iran (www.tahaghaleb.com).

References

1. Lee TC, Chan LC, Zheng PF (1997) Application of the finite-element deformation method in the fine blanking process. J Mater Process Technol 63(1–3):744–749 doi:10.1016/S0924-0136(96)02717-3
2. Faura F, García A, Estrems M (1998) Finite element analysis of optimum clearance in the blanking process. J Mater Process Technol 80–81:121–125 doi:10.1016/S0924-0136(98)00181-2
3. Brokken D, Brekelmans WAM, Baaijens FPT (1998) Numerical modeling of the metal blanking process. J Mater Process Technol 83(1–3):192–199 doi:10.1016/S0924-0136(98)00062-4
4. Samuel M (1998) FEM simulations and experimental analysis of parameters of influence in the blanking process. J Mater Process Technol 84(1–3):97–106 doi:10.1016/S0924-0136(98)00083-1
5. Chen ZH, Tang CY, Lee TC, Chan LC (1998) A study of strain localization in the fine-blanking process using the large deformation finite element method. J Mater Process Technol 86(1–3):163–167 doi:10.1016/S0924-0136(98)00306-9
6. Pyttel T, John R, Hoogen M (2000) Finite element based model for the description of aluminum sheet blanking. Int J Mach Tools Manuf 40(14):1993–2002 doi:10.1016/S0890-6955(00)00043-2
7. Maiti SK, Ambekar AA, Singh UP, Date PP, Narasimhan K (2000) Assessment of influence of some process parameters on sheet metal blanking. J Mater Process Technol 102(1):249–256 doi:10.1016/S0924-0136(99)00486-0
8. Klocke F, Sweeney K, Raedt HW (2001) Improved tool design for fine blanking through the application of numerical modeling technique. J Mater Process Technol 115(1):70–75 doi:10.1016/S0924-0136(01)00771-3
9. Fang G, Zeng P, Lou L (2002) Finite element simulation of the effect of clearance on the forming quality in the blanking process. J Mater Process Technol 122(2–3):249–254 doi:10.1016/S0924-0136(02)00056-0
10. Rachik M, Roelandt JM, Maillard A (2002) Some phenomenological and computational aspects of sheet metal blanking simulation. J Mater Process Technol 128(1–3):256–265 doi:10.1016/S0924-0136(02)00460-0
11. Aoki I, Takahashi T (2003) Material flow analysis on shearing process by applying Fourier phase correlation method—analysis of piercing and fine blanking. J Mater Process Technol 134(1):45–52 doi:10.1016/S0924-136(02)00917-2
12. Klingenberg W, Singh UP (2003) Finite element simulation of the punching/blanking process using in-process characterization of mild steel. J Mater Process Technol 122(3):296–302 doi:10.1016/S0924-0136(02)01113-5
13. Brokken D (1999) Numerical modeling of ductile fracture in blanking. Ph.D. thesis, Eindhoven University of Technology, the Netherlands
14. Lemaitre J (1985) Local approach of fracture. Eng Fract Mech 25 (5–6):523–537 doi:10.1016/0013-7944(86)90021-4
15. Goijaerts AM, Govaert LE, Baaijens FPT (2002) Experimental and numerical investigation on the influence of process speed on the blanking process. J Manuf Sci Eng Trans ASME 124(2):416–419
16. Hambli R, Reszka M (2002) Fracture criteria identification using an inverse technique method and blanking experiment. Int J Mech Sci 44(7):1349–1361 doi:10.1016/S0020-7403(02)00049-8
17. Shim KH, Lee SK, Kang BS, Hwang SM (2004) Investigation on blanking of thin sheet metal using the ductile fracture criterion and its experimental verification. J Mater Process Technol 155–156 (1–3):1935–1942 doi:10.1016/j.jmatprotec.2004.04.284
18. Cockcroft MG, Latham DJ (1968) Ductility and the workability of metals. J Inst Met 96:33–39

19. Komori K (2005) Ductile fracture criteria for simulating shear by node separation method. Theor Appl Fract Mech 43(1):101–114 doi:10.1016/j.tafmec.2004.12.006
20. Yu S, Xie X, Zhang J, Zhao Z (2007) Ductile fracture modeling of initiation and propagation in sheet-metal blanking processes. J Mater Process Technol 187–188:169–172 doi:10.1016/j.jmatprotec.2006.11.179
21. Brozzo P, Deluca B, Rendina R (1972) A new method for the prediction of formability limits in metal sheets. Sheet metal forming and formability. In: Proceedings of the Seventh Biannual Conference of the International Deep Drawing Research Group
22. Lestriez P, Saanouni K, Mariage JF, Cherouat A (2004) Numerical prediction of ductile damage in metal forming processes including thermal effects. Int J Damage Mech 13(1):59–80 doi:10.1177/1056789504039257
23. Chen ZH, Tang CY, Lee TC (2004) An investigation of tearing failure in fine-blanking process using coupled thermo-mechanical method. Int J Mach Tools Manuf 44(2–3):155–165 doi:10.1016/j.ijmachtools.2003.10.010
24. Freudenthal AM (1950) The inelastic behavior of engineering materials and structures. Wiley, New York
25. Rice JR, Tracey DM (1969) On the ductile enlargement of voids in triaxial stress fields. J Mech Phys Solids 17:201–217 doi:10.1016/0022-5096(69)90033-7
26. Oyane M, Sato T, Okimoto K, Shima S (1980) Criteria for ductile fracture and their applications. J Mech Working Technol 4:65–81 doi:10.1016/0378-3804(80)90006-6
27. Goijaerts AM (1998) Prediction of ductile fracture in metal blanking, Ph.D. thesis, Eindhoven University of Technology, Netherlands
28. Scientific Forming Technologies Corporation (2004) DEFORM2D user's guide, version 8.1. Scientific Forming Technologies Corporation.
29. Kobayashi S, Oh SI, Altan T (1989) Metal forming and the finite element method. Oxford University Press, Oxford
30. Goijaerts AM, Govaert LE, Baaijens FPT (2000) Prediction of ductile fracture in metal blanking. J Manuf Sci Eng Trans ASME 122(2):476–483
31. Mediavilla J, Peerlings RHJ, Geers MGD (2006) An integrated continuous-discontinuous approach towards damage engineering in sheet metal forming processes. Eng Fract Mech 73(7):895–916 doi:10.1016/j.engfracmech.2005.10.011